CONTRIBUTIONS OF ACTIVE SITE RESIDUES TO SUBSTRATE BINDING AND CATALYSIS OF 5-NITROANTHRANILIC ACID AMINOHYDROLASE

A Thesis
Presented to
The Academic Faculty

by

Xingjian Tao

In Partial Fulfillment
of the Requirements for the Degree
M.S. Chemistry in the School of
Chemistry & Biochemistry

Georgia Institute of Technology

May 2019

CONTRIBUTIONS OF ACTIVE SITE RESIDUES TO SUBSTRATE BINDING AND CATALYSIS OF 5-NITROANTHRANILIC ACID AMINOHYDROLASE

Approved by:

Dr. Raquel Lieberman, Advisor
School of Chemistry and Biochemistry
Georgia Institute of Technology

Dr. Vinayak Agarwal
School of Chemistry and Biochemistry
Georgia Institute of Technology

Dr. Amit Reddi
School of Chemistry and Biochemistry
Georgia Institute of Technology

Date approved: April 11th, 2019

ACKNOWLEDGEMENTS

I would like to thank my principal investigator Dr. Raquel Lieberman for her guidance and support. In addition, I would like to thank Dr. Swe-Htet Naing and Dr. Sibel Kalyoncu for their mentoring and contribution towards the foundation of my project. I would like to thank Dr. Verna Frasca from Malvern Panalytical for her support. I would also like to thank current members of Lieberman Lab: Dr. Shannon Hill, Dr. Dustin Huard, and Dr. Athéna Patterson Orazem for the support and laughter they brought to the lab. I would like to thank my thesis committee members, Dr. Vinayak Agarwal and Dr. Amit Reddi. I would also like to acknowledge the Argonne National Laboratory for their support throughout the course of the project. Again, to all the members of Lieberman lab and friends in chemistry department, past and present, I sincerely thank you for your support and friendship that will always be a part of my Georgia Tech experience.

TABLE OF CONTENTS

LIST OF TABLES

LIST OF FIGURES

LIST OF SYMBOLS AND ABBREVIATIONS

SDM	Site Directed Mutagenesis
LB	Luria Broth
IPTG	isopropyl-β-D-1-thiogalactopyranoside
EDTA	Ethylenediaminetetraacetic acid
GF	Gel filtration
Sup75	Superdex 75 GF column
AMP	Ampicillin
KAN	Kanamycin
SDS-PAGE	Sodium Dodecyl Sulfate Polyacrylamide Gel Electrophoresis
WT	Wild Type
Southeast Regional Collaborative Access Team	SER-CAT

SUMMARY

Synthetic and naturally occurring nitroaromatic compounds are recalcitrant to degradation and they are toxic/mutagenic. The symbiont *Bradyrhizobium* sp. JS329 is the first microbe found to degrade a biological nitroaromatic compound, 5-nitroanthralinic acid (5NAA), which is secreted by the bacterium responsible for potato scabs, *Streptomyces scabies*. The first enzyme in the degradation pathway is 5NAA-aminohydrolase (5NAA-A), a metalloprotease family member that has evolved to hydrolyze 5NAA to 5-nitrosalicylic acid. 5NAA-A is the first characterized metalloenzyme to utilize nucleophilic aromatic substitution. Here, I used isothermal titration calorimetry, enzyme activity assays, and X-ray crystallography to dissect contributions of individual active site and second-shell residues for assisting substrate transport. My studies demonstrate the interplay between substrate binding and catalysis requirements for this unusual metalloenzyme. Knowledge of the 5NAA-A structure and mechanism informs potential bioremediation and biocatalytic approaches to mitigate the environmental and ecological impact of nitroaromatic and other challenging substrates.

CHAPTER 1

INTRODUCTION TO 5-NITROANTHRONILLIC ACID

1.1 Biodegradation of nitro-aromatic compounds

Nitro-aromatic compounds are widely used as dyes, synthetic intermediates, and explosives, which are generally toxic, suspected carcinogens, and difficult to degrade[1]. Remarkably, bacteria from areas contaminated with synthetic nitroaromatics can use several industrial nitroaromatic compounds such as nitrobenzene, nitrophenols, and nitrotoluenes as carbon, nitrogen, and energy sources for growth[18]. Detailed studies have revealed that the general strategy used to metabolize nitroaromatic compounds is first to convert substrate to substituted phenols, quinones, or catechols, which are then metabolized to intermediates of the tricarboxylic acid (TCA) cycle[18]. By contrast, in the lab, nitrobenzene can be degraded into phenol in two chemical steps. First nitrobenzene is reduced using strong acid and catalyst to generate aniline, and then the aniline is treated with sodium nitrite and acid in cold condition to form benzene diazonium chloride, which on further treatment with water gives phenol.

Over 200 natural nitroaromatic compounds are produced by a variety of microbes, plants, and animals[2], but little is known about their biodegradation mechanisms. Rhizospheric bacteria that live on and near the roots of plant have been shown to contribute to the biodegradation of naturally-occurring aromatic compounds in contaminated plant soil[3]. For example, such bacteria can survive in the presence of *Streptomyces scabies*, which causes potato scab[4-5], an agriculture disease of worldwide economic importance[6]. The primary *Streyptomyces scabies phytotoxin is thaxtomin, which is a* 5-nitrotryptophan-containing cyclic dipeptide[7]. An additional metabolite secreted by *S. scabies,* 5-nitroanthranilic acid (5NAA) (Figure 1a.), was found to be

degraded by *Bradyrhizobium* sp. JS329, a rhizospheric bacterial strain isolated from potato field soil[8]. By eliminating the 5NAA metabolite of the *S. scabies* chemical arsenal, *Bradyrhizobium* sp. JS329 presumably protects itself and plants from disease[3].

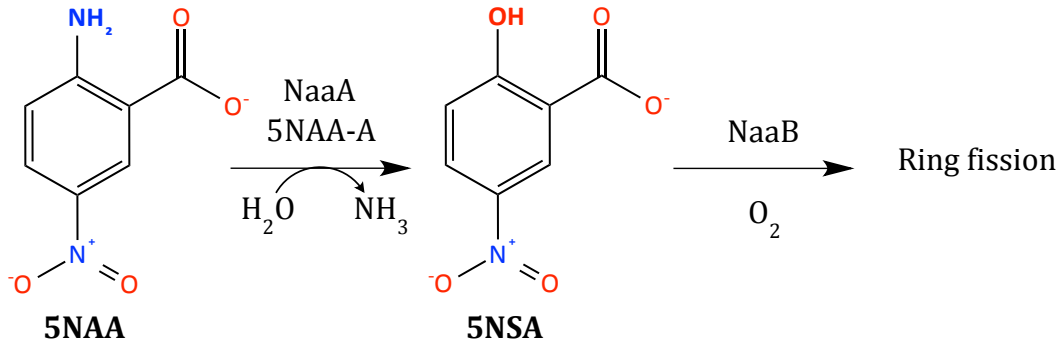

Figure 1: Chemical transformation of 5NAA to 5NSA catalyzed by 5NAA-A.

Bradyrhizobium JS329 was isolated from soil by our collaborator, Jim C. Spain (Georgia Tech), using a process involving selective enrichment with 5NAA[8]. Dr. Spain found that the bacterial isolate released stoichiometric amounts of nitrite and half of the stoichiometric amounts of ammonia when grown on 5NAA, and 5-nitrosalicylic acid (5NSA) was generated as intermediate. This transformation is a deamination reaction catalyzed by aminohydrolase (5NAA-A) to produce the 5NSA intermediate (Figure 1), followed by an unusual ring fission dioxygenation prior to removal of the nitro group[4]. Bioinformatics studies showed that the genes involved in 5NAA degradation were localized on a 40-kb fosmid[8], and naaA gene encoding 5NAA-A is related to the amino acid sequences of M20 metalloprotease group containing metal-binding residues[8].

1.2 Overall structure of 5NAA-A and its substrate binding sites

To understand the mechanism of hydrolysis of 5NAA by 5NAA-A, X-ray crystallographic and biochemical studies of 5NAA-A and key mutants were conducted by a previous graduate student, Dr. Sibel Kalyoncu. The crystal lattice and solution small

angle X-ray scattering confirm an octameric arrangement in which the eight ~43-kDa 5NAA-A protomers are arranged around a ~50–Å-diameter solvent channel (Figure 2a, top) to form a ~350-kDa enzyme[7]. Loop configurations generate two large surface areas: a dimerization interface, and tetramerization interface (Figure 2a, top). The dimerization interface contains the 5NAA-A catalytic center (Figure 2a, bottom), which is confirmed by finding that the V247K variant, designed to destabilize this interface, could not be purified to appreciable levels[7]. Loop one and two disordered in the apo structure are located in this region of the catalytic lobe, and become organized upon binding of substrate[7] (Figure 2b).

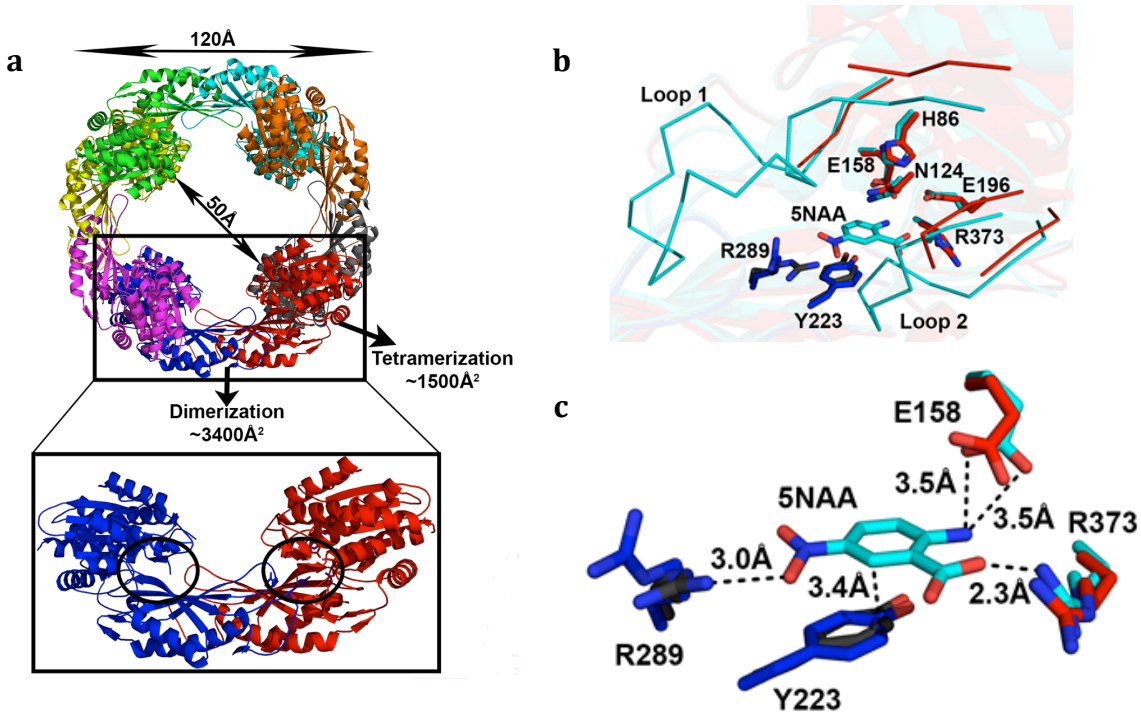

Figure 2: Overall structure and substrate binding features of 5NAA-A. (a) Top, octameric crystal structure of 5NAA-A, colored by protomer (apo structure shown). Bottom, dimer unit labeled with location of two active sites. (b) Substrate binding details. superposition of apo and 5NAA-bound structures in binding pocket. Loop 1 (residues 91–108) and loop 2 (residues 393–397) are disordered in the apo structure (red and dark blue) but adopt an ordered conformation when 5NAA is bound (cyan and gray). (c) 5NAA binding interactions with protein residues, superimposed with apo structure[7].

The crystal structure of 5NAA-A with bound 5NAA substrate reveals that the

5NAA substrate bound at catalytic pocket is stabilized by Tyr223 (Y223) (Figure 2c), which provides π-π stacking stabilization to substrate and Arg289 (Figure 2c), which stabilizes the nitro group of 5NAA[7]. Within the catalytic lobe, the carboxyl group of 5NAA is stabilized by Arg373 (Figure 2c), and Glu158 (Figure 2c) is found to be within hydrogen bonding distance of the amino substituent[7]. The crystal structure of 5NAA-A with the product 5NSA and Mn^{2+} reveal that metal is bound by a triad of residues His86, Glu196, and Asn124 (Figure 2b), adjacent to the substrate/product-binding pocket. Combined with reported crystal structures of Meisenheimer complex of Zn^{2+} bound to the 5NAA-A R289A mutant[7], the hydrolysis of 5NAA is postulated to be a nucleophilic aromatic substitution mechanism[7](Figure 3).

The hydrolysis of 5NAA is an unusual case of nucleophilic aromatic substitution for two reasons. First, most aminohydrolases act upon aliphatic amines, changing them to aliphatic alcohols[9]. However, 5NAA-A deaminates an aromatic amine (5NAA), producing a phenol (5NSA). Second, as a metalloprotease, unlike typical metalloenzymes that have at least nanomolar affinity for metal ions[10], 5NAA-A has weak affinity for metal ions, but metal ions are required in the hydrolysis of 5NAA substrate[7].

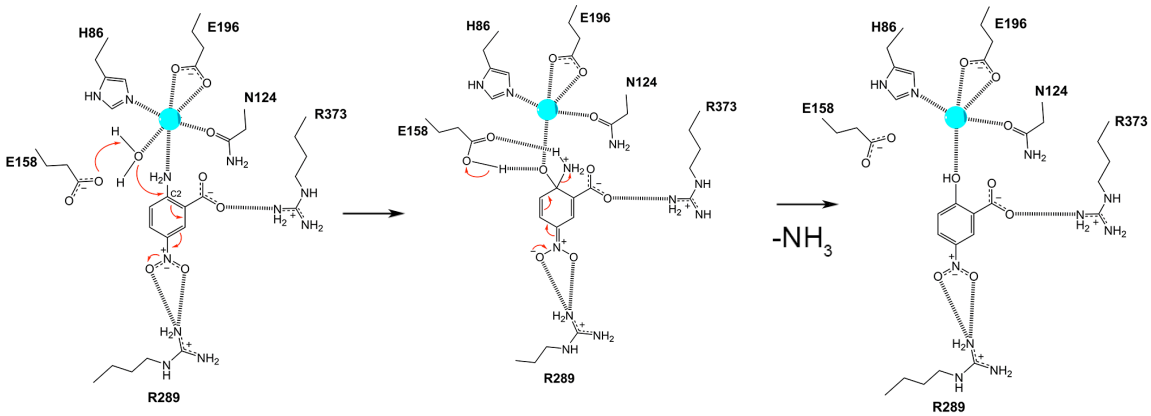

Figure 3: Proposed nucleophilic aromatic substitution mechanism for hydrolysis of 5NAA to 5NSA by 5NAA-A.

Although 5NAA-A has weak affinity for metal ions, the substrate 5NAA has a high apparent affinity for Zn^{2+} based on competition assay with Indo-1, a sub-nanomolar fluorescent chelator of Zn^{2+} [7]. The crystal structure of 5NAA with Zn^{2+}, solved by John Basca with assistance from Henry LaPierre, shows that Zn^{2+} coordinates at the carboxyl group of 5NAA in a 1:2 ratio (Figure 4), which is different from the coordination environment in the substrate-bound protein crystal structure in which Zn^{2+} coordinates at the amino group of 5NAA-A and the carboxyl group is stabilized by Arg373 (Figure 3). The electron-withdrawing nitro group on 5NAA likely causes the *para*-amino substituent to be a weak ligand, so that metal ion complexation in solution instead involves the carboxylate substituent.

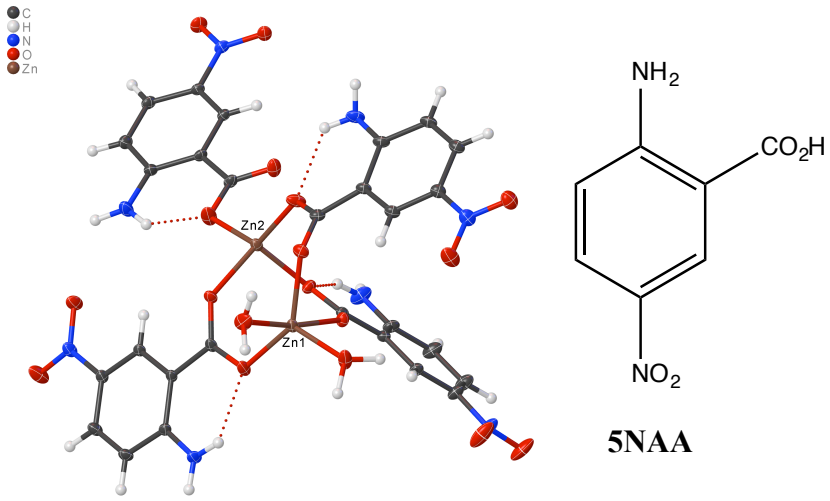

Figure 4: Crystal structure of 5NAA and Zn^{2+}. (Crystallized by Henry LaPierre, structure solved by John Basca)

A major open question about 5NAA-A, which this thesis addresses, is how the metal-bound substrate binds to 5NAA-A. Comparison of the coordination environment in the absence and presence of 5NAA-A, it is clear that a major reorganization is required to convert from the observed substrate and metal configuration to that seen within the

5NAA-A active site[7]. Since two R289 and R373 play key roles in stabilizing 5NAA in 5NAA-A, in this thesis, I hypothesize that arginine residues on loop 1 (Figure 5), which are adjacent to substrate binding sites, stabilize the nitro group of the 5NAA substrate along its path to the catalytic pocket of 5NAA-A. There are three arginine residues (R93, R98, and R105) located on loop 1 of 5NAA-A (Figure 5). The closest one to active site, R98, appears most likely to perform this role.

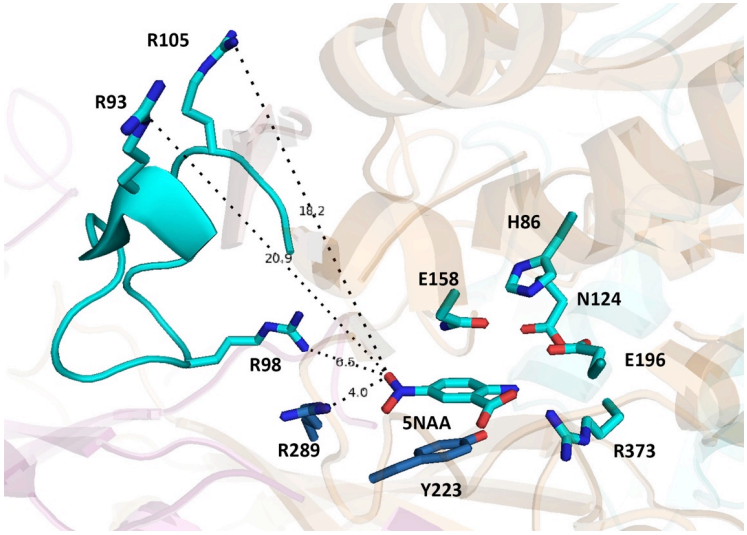

Figure 5: Positions of arginine residues on loop 1 (residues 91–108).

CHAPTER 2

EXPERIMENTAL METHODS

2.1 Expression of 5NAA-A

5NAA-A was cloned previously into the pET-30 Xa/LIC vector (Novagen), which contains His tag and S tag coding sequences that are cleavable with Factor Xa protease. Wild-type 5NAA-A was expressed in *E. coli* Rosetta 2 cells. A single transformed colony was inoculated into a selective 200 mL Luria-Bertani culture (LB, Fisher, supplemented with 34 μg/mL chloramphenicol, 50 μg/mL kanamycin) and agitated overnight (16–18 h), 37 °C, 225 r.p.m. A starter culture (20 mL) was used to inoculate 1 L of selective LB media, which was then agitated at 37 °C, 225 r.p.m. until an optical density at 600 nm of 1.0 was reached. The cell cultures were cooled to 25 °C, with shaking at 225 r.p.m. for 1 h, then induced with 0.5 mM isopropyl β-d-1-thiogalactopyranoside (IPTG, Calbiochem), and allowed to grow overnight (16–18 h) at 25 °C, shaking at 225 r.p.m. Grown cells were pelleted (5,000 × g, 10 min, 4 °C) and subsequently flash-frozen with liquid nitrogen and stored at −80 °C[7].

5NAA-A variants (H86A, E158A, R289A, Y223A) were generated previously by SDM (QuikChange Lightning Kit, Agilent Technologies) using the WT 5NAA-A as the template and confirmed by sequencing; I used the same method to generate R98A (Table 1). Expression and purification was accomplished as described in the previous section.

Table 1: 5NAA-A R98A primers.

Mutation	Primers
R98A	Forward: 5’-cgcgaggacacggcggcgtttgcggatgcg -3’
	Reverse: 5’-cgcatccgcaaacgccgccgtgtcctcgcg -3’

2.2 Purification of 5NAA-A variants

Cell pellets of E. coli expressing 5NAA-A were thawed and suspended in Ni^{2+}-affinity purification wash buffer (50 mM HEPES pH 7.5, 500 mM NaCl, 40 mM imidazole, 10% glycerol) containing 0.5mL Roche Complete EDTA-free Protease Inhibitor and lysed by two passages through a French Press (13,000 psi). Cellular debris of E. coli expressing 5NAA-A was removed by ultracentrifugation (40,000 × g, 45 min, 4 °C). The supernatant was collected and loaded onto a 1 mL Ni^{2+} affinity purification column (GE Healthcare) on an AKTA FPLC system (GE Healthcare) equilibrated with wash buffer. After sample loading and washing to remove unbound proteins, 5NAA-A was eluted with a gradient from 40–500 mM imidazole. Fractions containing 5NAA-A were collected and concentrated using an Amicon 30K MWCO filter (EMD Millipore) and exchanged into Factor Xa cleavage buffer (50 mM Tris pH 7.5, 100 mM NaCl, 5 mM $CaCl_2$). In order to exclude the binding of metal ions to the N-terminal hexa-histidine tag, the tag was removed by incubation with Factor Xa (Roche, 50:1 mass ratio) for 20 hours at 4 °C. Subsequently, the digested mixture was re-loaded onto 1 mL Ni^{2+} affinity purification column, and the flow-through fractions containing 5NAA-A were concentrated in an Amicon 30K MWCO filter. The final polishing step was accomplished by loading the concentrate onto a HiLoad 16/60 Superdex 75 prep grade column (GE Healthcare) equilibrated with gel filtration buffer (50 mM Bicine pH 7.0, 150 mM NaCl). The fractions containing pure 5NAA-A were concentrated in an Amicon 30K MWCO filter for experiments. Purity of 5NAA-A protein was assessed by 12% SDS–PAGE analysis with Coomassie staining. Concentration was measured using a NanoDrop spectrophotometer (ThermoScientific, ε = 74,461.88 M^{-1} cm^{-1} for 5NAA-A determined

by total amino acid analysis (Molecular Structure Facility, University of California, Davis) and calculated molecular weight was determined from respective amino acid sequences for a monomer[7].

2.3 Isothermal titration calorimetry

Freshly purified WT 5NAA-A and variants were prepared in gel filtration buffer at 11.1 μM in 1.8 ml aliquots. For the ligand, stock solution of 1 mM 5NAA was diluted to 0.15 mM with gel filtration buffer. Before ITC binding experiments (MicroCal VP-ITC), both 5NAA-A enzymes and substrate samples were degassed on a vacuum line (MicroCal ThermoVac). In a typical experiment, an automated sequence of 31 injections of 9μL of sample was applied to the protein in the sample cell with 300 sec interval between injections to allow for equilibration. The reaction solution was stirred at 270 r.p.m, and the temperature of the chamber was maintained at 25 °C. Calibration run using 0.1 mM EDTA to 1 mM $CaCl_2$ was performed before ITC experiment. ITC data was analyzed with the Origin 7.0 software package from MicroCal. The one-site binding model was used to best fit parameters for the number of binding sites (n), the association constant (K_a) and the change in enthalpy ($\Delta H°$). The dissociation constant (K_d) was calculated by taking the inverse of K_a. Experiments were conducted by increasing protein concentration to adjust the c value ($c = n \bullet Ka \bullet [titrand]$) to optimize curve shape of ITC. Decreasing injection volume and increasing injection time was adjusted to delay the saturation rate of protein during experiments. Post-experiments analysis was assisted by Verna Frasca from Malvern Panalytical.

2.4 Enzyme activity assay

To assess the activity of 5NAA-A variants after purification, a spectrophotometric

assay was used, which follows the depletion of substrate (λ_{max} for 5NAA = 374 nm; λ_{max} for 5NSA = 306 nm)[7]. 5NAA (100μM) and zinc chloride (500μM) were mixed with freshly purified 5NAA-A enzyme (0.25μM) in gel filtration buffer (100 L total volume). The reaction mixture was mixed on ice by gentle pipetting, and LAMBDA XLS spectrophotometer was used to record absorbance readings every 3 min for 2 h. 5NAA depletion (374 nm) and 5NSA (306nm) generation were used for data analysis. After purification, mass spectrometry analysis was conducted at the Georgia Institute of Technology Bioanalytical Mass Spectrometry Facility by Electrospray ionization (ESI). For each sample, a buffer was fused with the sample to subtract the contribution of the buffer from the sample spectrum.

2.5 Co-crystallization of 5NAA-A variants and substrate

Crystallization trials: Apo-5NAA-A crystals were grown by using the sitting-drop method at room temperature in sodium cacodylate and trisodium citrate as previously published[7], with slight optimization. 5NAA-A Y223A and R98A crystals (7 mg/mL protein in 50 mM Bicine pH 7.0, 150 mM NaCl) were grown by the sitting-drop method at room temperature in 0.1 M sodium cacodylate pH 6.5, and trisodium citrate (0.55 M - 1.05 M). For looping, crystals of Y223A and R289A were cryo-cooled in a solution containing the corresponding reservoir solution supplemented with 20% glycerol.

X-ray data collection and structure determination: Diffraction data were collected at beamline 22-ID of the Southeast Regional Collaborative Access Team (SER-CAT) at the Advanced Photon Source, Argonne National Labs. Data were indexed, integrated, scaled and processed using XDS[12]. The initial structures of Y223A were solved by

molecular replacement using Phaser[13], using R289A-bound 5NAA-A structure as a search model (PDB: 5K8N). The models were iteratively built and refined using Coot[14] and phenix.refine[15]. eLBOW[16] within PHENIX was used to generate ligand restraints of 5NAA, and Readyset[16] within PHENIX was used to generate metal coordination restriants of zinc metal ions.

CHAPTER 3

RESULTS

3.1 Characterization of metal binding residues

A triad of metal binding residues, in the 5NAA-A enzyme, H86-E196-N124 was previously identified[7]. In order to investigate the effect of these residues in binding 5NAA in the catalytic pocket, the alanine mutant of H86, and aspartate mutant of N124 were generated and purified for further characterization[7] (Figure7). Both H86A and N124D are not active[7].

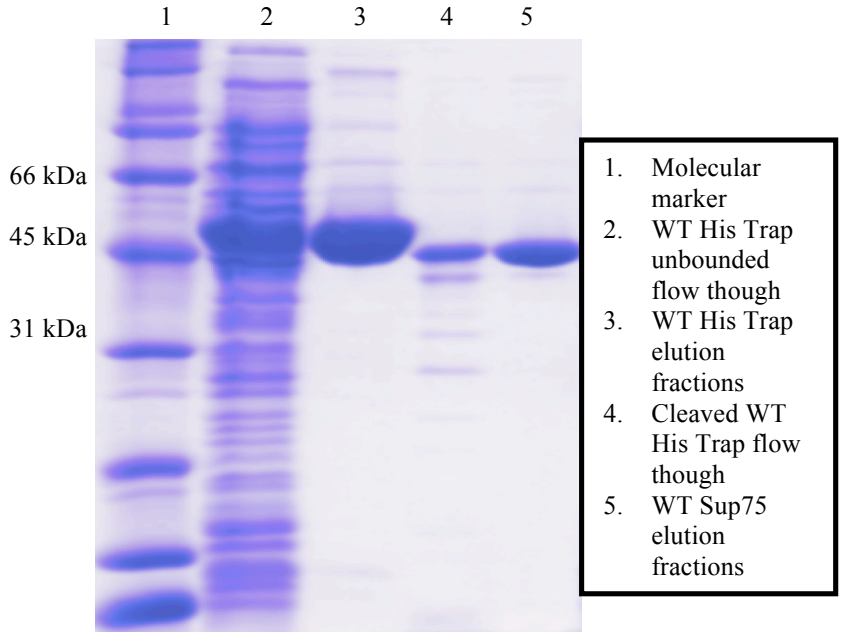

Figure 6: Gel image of purified 5NAA-A WT.

3.1.1 5NAA binding to H86A variant

After expression and purification, the purity of H86A was assessed by SDS-PAGE (Figure 7) and then used for ITC measurements. Binding of H86A variant to 5NAA is similar to that seen for wild-type 5NAA-A (Figure 8a, K_d = 1.19 ± 0.058 μM, stoichiometry value of 1.05). This result indicates that mutation at metal binding motif

would not affect substrate binding.

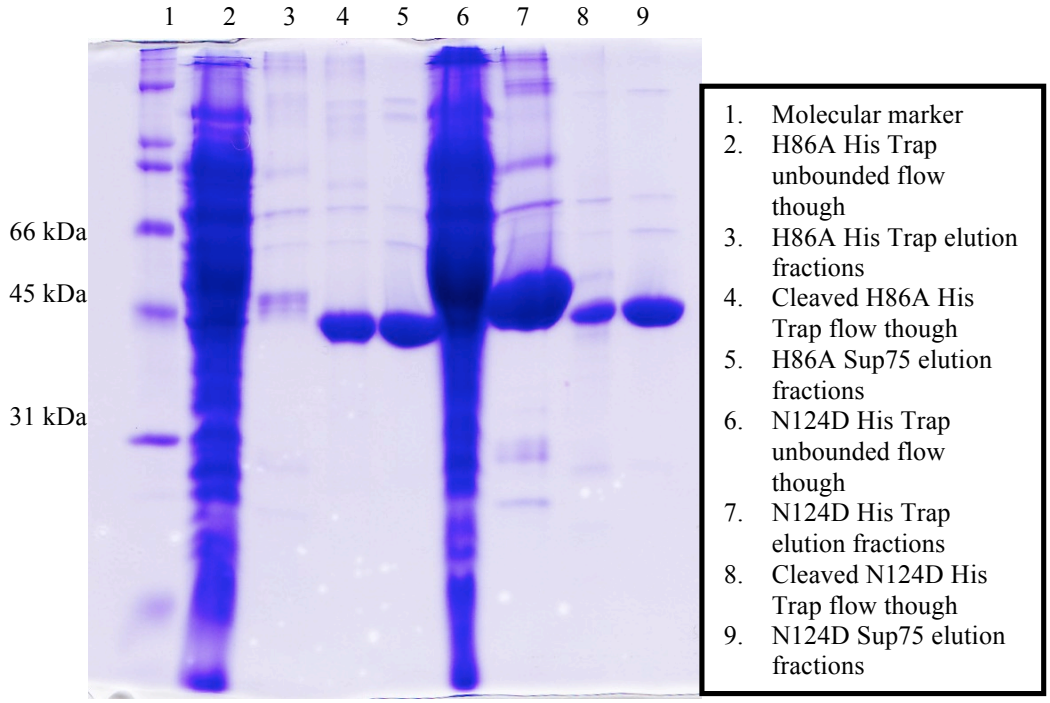

Figure 7: Gel image of purified 5NAA-A H86A and N124D.

3.1.2 5NAA binding to N124D variant

N124D modifies the asparagine into aspartic acid, which contains negatively charged side chain that metal ions prefer to bind to. 5NAA N124D mutant enzyme was then purified, checked for purity by SDS-PAGE (Figure 7), and used for ITC experiments. Affinity between 5NAA and N124D (Figure 8c) revealed similar binding affinity (K_d = 1.34 ± 0.285 uM) to that of wild-type 5NAA-A (K_d = 1.19 ± 0.058 μM) and stoichiometry value of 0.246 suggested that mutation of metal binding residue N124 would not affect substrate binding affinity but would impact 5NAA-A's occupancy.

It proved very challenging to get a sigmoidal curve for 5NAA binding to N124D, indicating its low stability in the ITC sample chamber. Several variables, including injection volume, enzyme concentration, ligand concentration, and time between

injections were modified to optimize ITC results. In some trials, a robust heat change (~40 μcal) was observed for the first two injections, but the curve appeared non-sigmoidal, indicating that the enzyme was not driven to saturation. In order to make enzyme saturation later in the titration curve, the concentration of 5NAA in the syringe was decreased by ~2 fold and keep the same protein concentration in the cell. The method serves to drive the enzyme saturation and to decrease the heat change per injection.

In some trials, the baseline did not return to the pre-injection level during the first injections where binding was occurring. The reason could be that the time between injections was not enough so that injection peaks do not have enough time to go back to the baseline. Therefore, the time between injections was increased to up to 300 seconds in an attempt to allow the protein to reach equilibrium. Alternatively, the heat exchange per injection was lowered by decreasing injection volume of same concentration 5NAA from 10 μL to 5 μL. Both methods effectively improved data qualities.

Finally, low n values were obtained, compared to WT 5NAA-A where n equals close to 1. N is the stoichiometry ratio of enzyme to ligand or substrate, and it is possible that 5NAA-A in the ITC sample cell has a lower active concentration than the calculated concentration if N is lower than expected. The other possibility could be that ligand in the ITC syringe has a higher active concentration than calculated concentration. In Origin, the fitting software, we can still fit non-sigmoidal curves by assuming affinity is normal. In this case, the change of enthalpy is statistically extrapolated. Therefore, sometimes the N value is set to 1 to prevent it from floating during the curve fitting.

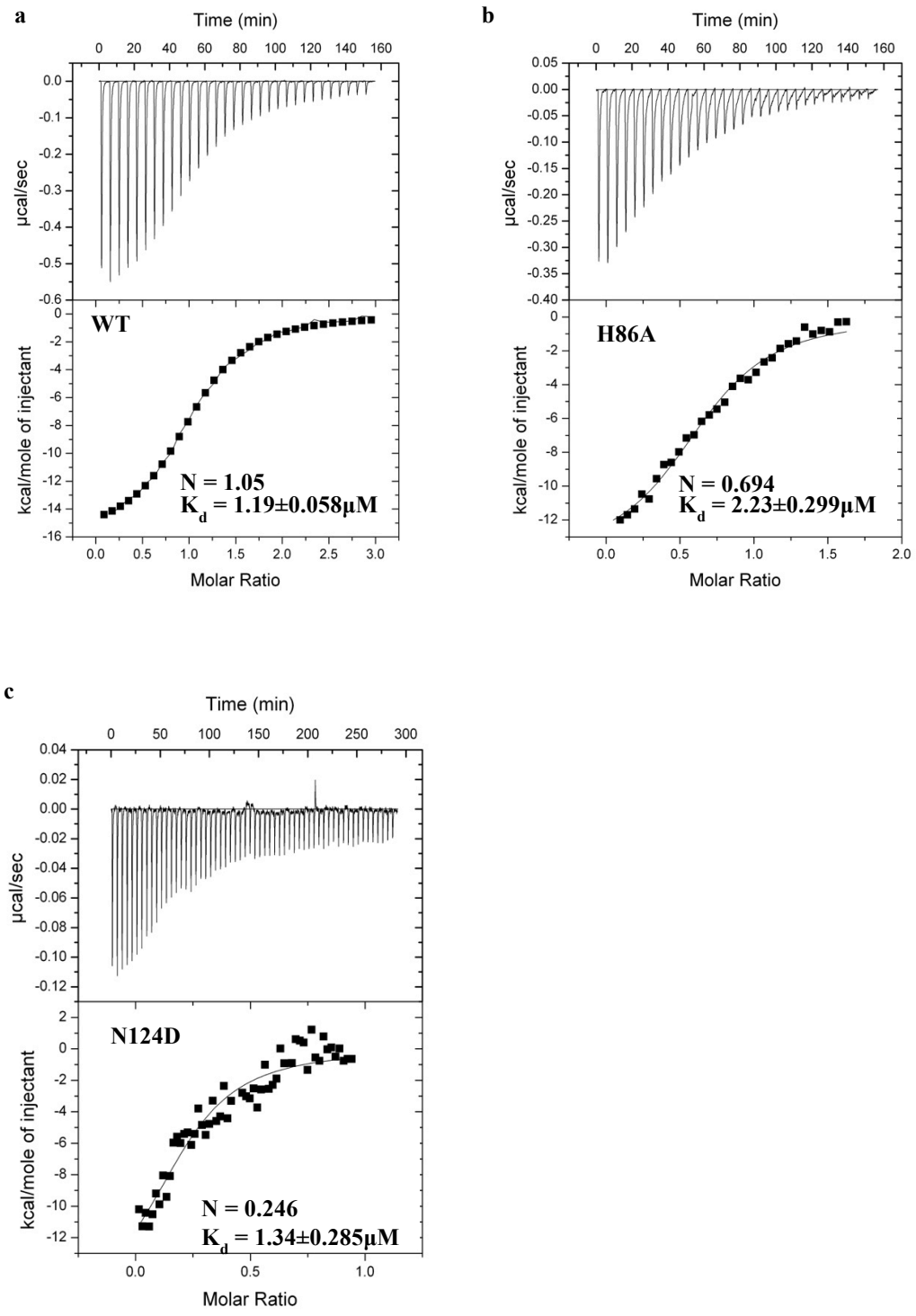

Figure 8: Substrate binding to 5NAA-A metal-binding mutants measured by ITC. Representative raw data and plot of integrated heat versus molar ratio with calculated Kd values. (a) 5NAA titrated to 5NAA-A WT, (b) 5NAA-A H86A, and (c) 5NAA-A N124D (Table 2).

Table 2: ITC data of 5NAA-A variants.

Residue Function	Mutants	ITC experimental parameters		Activity
		N	K_d (μM)	
Control	WT	1.05	1.19±0.058	Active
Loop one	R98A	0.533	1.66±0.139	Slow reaction
Catalysis	E158A	0.794	0.1±0.008	Inactive
Metal binding	H86A	0.694	2.23±0.299	Inactive
	N124D	0.246	1.34±0.285	Inactive
Substrate binding	Y223A	n/a	n/a	Inactive
	R289A	0.759	7.59±0.513	Half reaction
	R373A	0.565	5.03±0.566	Inactive

3.2 Characterization of substrate binding residues

Although key residues at catalytic pocket have been shown to bind 5NAA and Zn^{2+}, binding studies have not been conducted to clarify the energetic roles of each residue in binding the 5NAA substrate. To investigate details of substrate binding at catalytic pocket, ITC and structural studies were carried out on alanine variants of Y223, R289, R373, and E158. These were generated previously and tested to be inactive[7]. The purity of R289A, R373A, Y223A, and E158A was assessed by SDS-PAGE (Figure 9-12) and then directly used for ITC measurements.

3.2.1 5NAA binding to R289A variant

R289 is the residue that stabilizes the nitro substituent on 5NAA. After expression and purification (Figure 9), binding affinity between R289A and 5NAA was measured by ITC. Titrating 5NAA into R289A (Figure 13a) showed a K_d of 7.75±0.513μM and stoichiometry value of 0.759, indicating that 5NAA binds considerably more weakly

without the stabilizing interaction between the guanidinium group of R289 and the nitro group of the 5NAA.

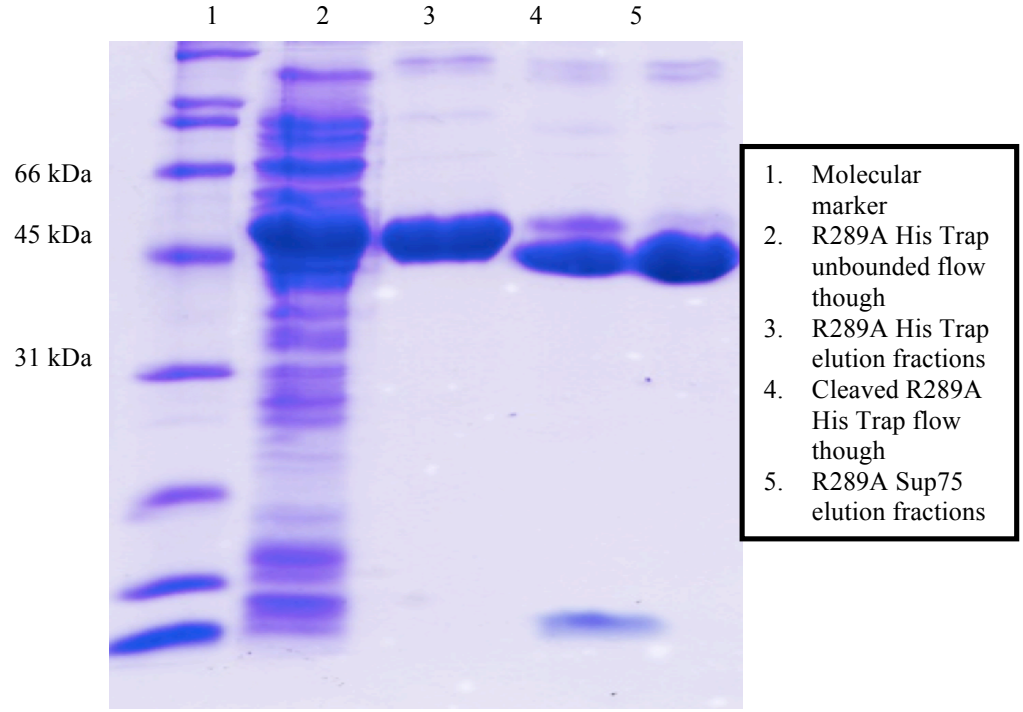

Figure 9: Gel image of purified R289A.

3.2.2 5NAA binding to R373A variant

R373 is the residue that stabilizes the carboxylic acid group. Similar to R289A, titrating 5NAA into R373A (Figure 13b) showed a weaker K_d value of 5.03±0.566μM. The stoichiometry was also closer to 0.5 than 1, suggesting that perhaps only half of the molecules in the 5NAA-A octamer can bind 5NAA in this variant.

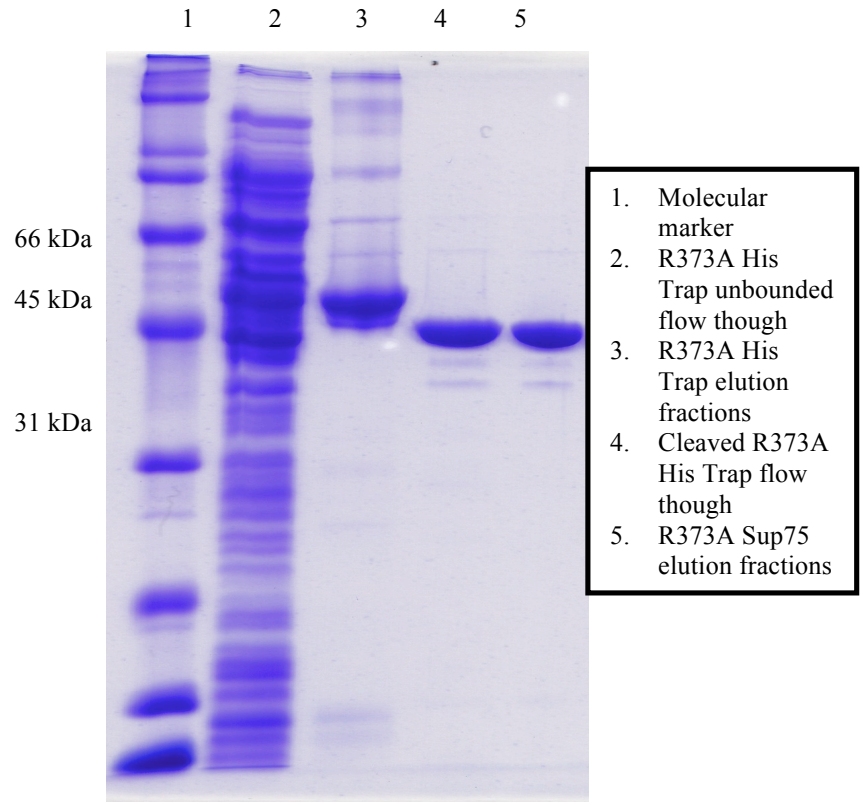

Figure 10: Gel image of purified R373A.

3.2.3 5NAA binding to E158A variant

At physiological pH, E158 would be fully active as a base, providing a localized negative charge. As expected, no detectable activity was observed in the enzymatic assay of E158A[7]. Unexpectedly, fitting curve of 5NAA to E158A (Figure 13d) showed a K_d of 0.1 ± 0.008 μM, which was lower than that of wild-type, implying that 5NAA binds tighter to the enzyme without the functional group E158. We propose this could be due to the removal of steric hindrance as well as the negatively charged carboxyl group, which would repel the negatively 5NAA substrate.

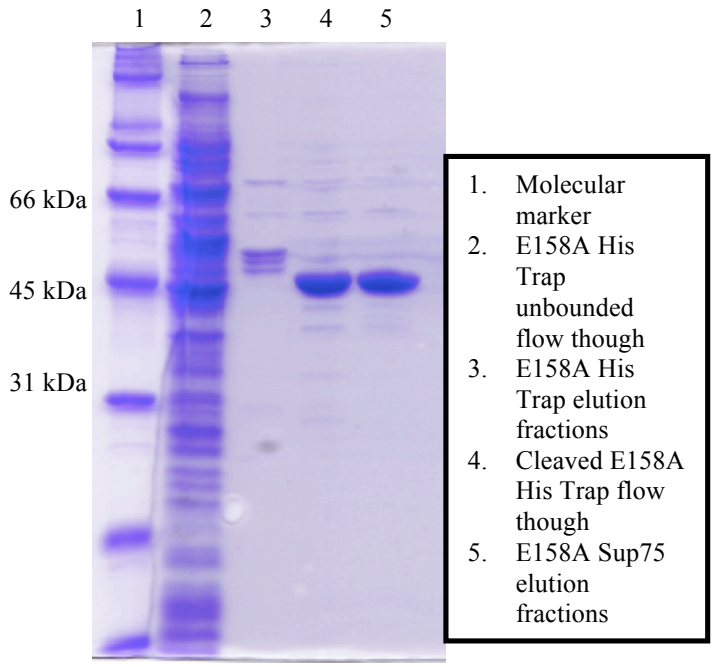

Figure 11: Gel image of purified E158A.

3.2.4 5NAA binding to Y223A variant

Y223 is the residue that forms a π-π stacking interaction with the substrate. Titrating 5NAA into Y223A (Figure 13c) revealed no heat of binding. This result suggests that 5NAA binding is below the detection limit of ITC.

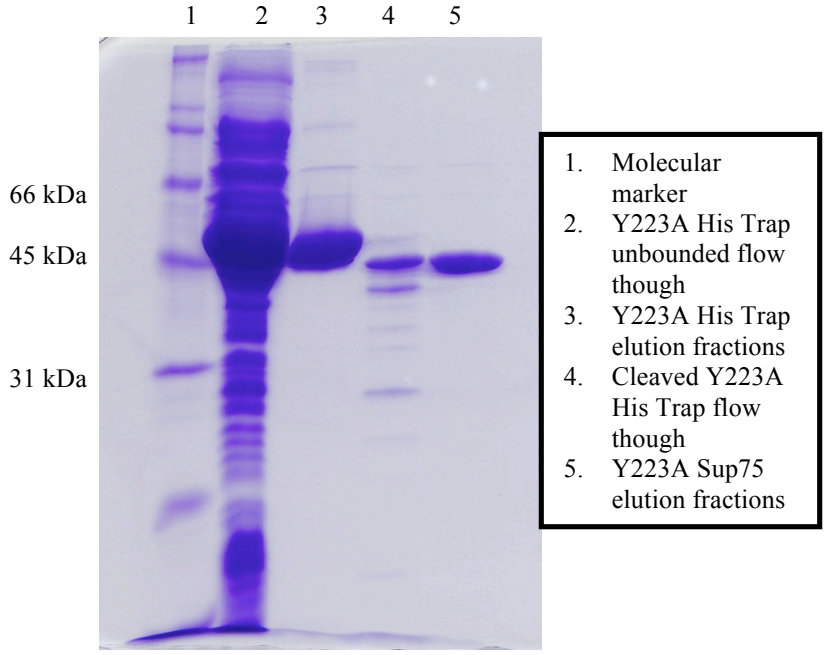

Figure 12: Gel image of purified Y223A.

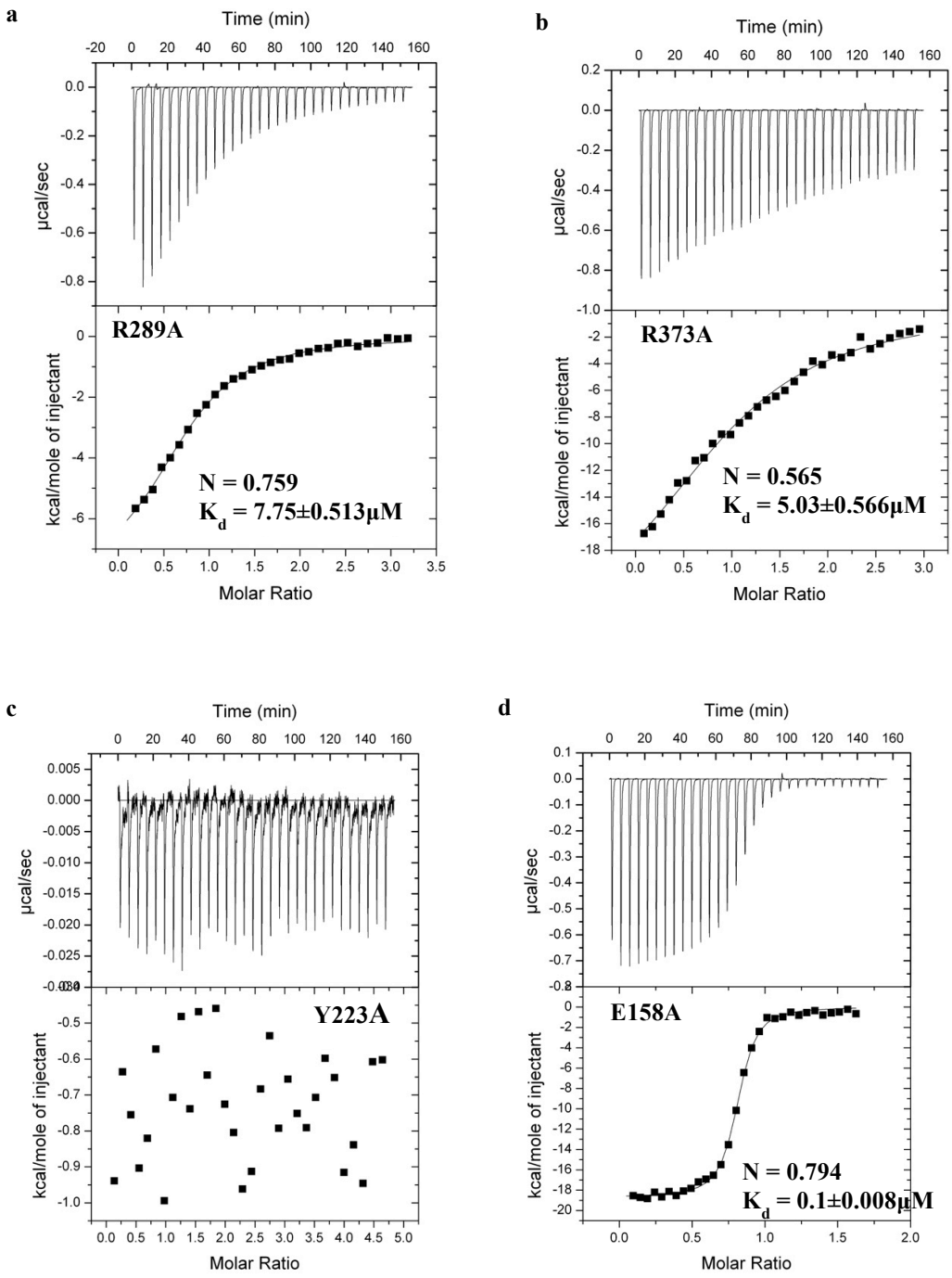

Figure 13: Substrate binding to 5NAA-A substrate-binding mutants measured by ITC. Representative raw data and plot of integrated heat versus molar ratio with calculated Kd values. (a) 5NAA titrated to 5NAA-A R289A, (b) 5NAA-A R373A, (c) 5NAA-A Y223A, and (d) 5NAA-A E158A.

3.2.5 Crystal structure of the Y223A variant in complex with 5NAA

The crystal structure of 5NAA in complex with Y223A was solved to 3.5 Å resolution (Supplementary Table 3). After identifying initial crystal growth conditions, crystallization trays were set up to optimize crystal quality. Factors such as protein concentration, precipitant concentrations, and additives were optimized for substrate-bound Y223A (Table 3).

Table 3: crystal tray setup of 5NAA with Y223A and R98A.

5NAA-A variant	Temperature	Concentration	Mother Liquour	Space group
Y223A	RT	7 mg/ml	0.1M sodium cacodylate pH 6.5, 0.65M trisodium citrate	$C2_12_12_1$ (orthorhombic)
R98A	RT	7 mg/ml	0.1 M sodium cacodylate pH 6.5, 0.67 M trisodium citrate	$C2_12_12_1$ (orthorhombic)

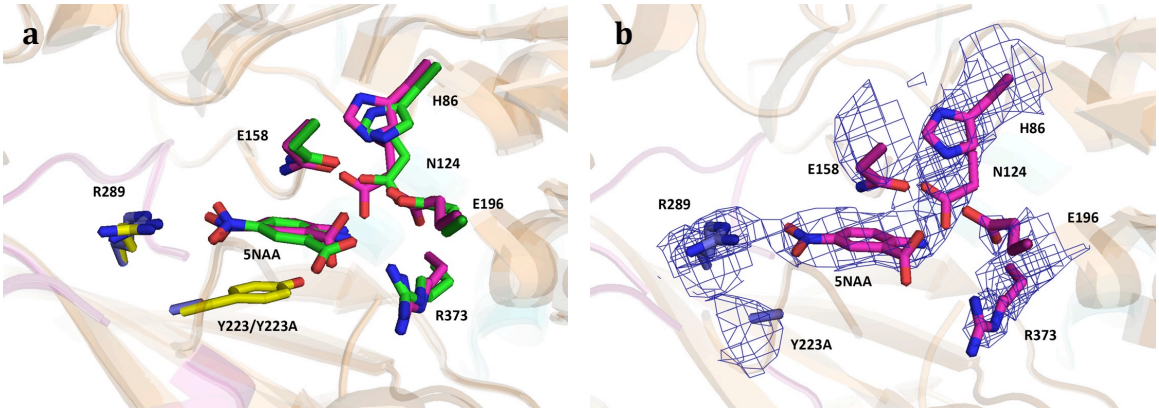

Figure 14: Structure of substrate coordination and electron density map of 5NAA-A Y223A complex. (a) Coordination environment and (b) Electron density for 5NAA-bound 5NAA-A Y223A. $2F_o - F_c$ electron density (blue) is contoured at 1.0 σ (Table 4).

Table 4. Collection, phasing, and refinement statistics of R98A and Y223A.

	5NAA-Y223A	**5NAA-R98A**
Data Collection		
Space group & File name	$C222_1$(02142018_ Y223A_gt12_pin8)	$C222_1$(06152018_ R98A_rrl5_pin11)
Cell dimensions		
a, b, c (Å)	185.54, 249.23, 248.78	185.12, 248.54, 248.78
α, β, γ (°)	90 90 90	90 90 90
Wavelength	1.00000 Å	1.00000 Å
Resolution (Å)	61.83 - 3.50 (3.63 - 3.50)	87.92 – 2.30 (2.38 – 2.30)
R_{sym}		
Completeness (%)	96.9	98.7
Refinement		
Resolution	61.83 - 3.50 (3.63 - 3.50)	87.92 – 2.30 (2.38 – 2.30)
No. of reflections	70341	248691
R_{work}/R_{free}	0.18/0.25	0.16/0.20
No. atoms		
Protein	25760	25799
Ligand/ion	104	112
B-factors		
Protein	53.4	31.7
Ligand/ion	71.5	39.7
R.m.s deviations		
Bond lengths (Å)	0.0142	0.0172
Bond angles (°)	1.41	0.94
Ramachandran		
Analysis		
Favored (%)	89.53	96.66
Outliers (%)	1.29	0.36

Crystallographic data of 5NAA with Y223A shows that the space group is C2 2 21, with one copy of the octamer per asymmetric unit. Refinement of Y223A and the 5NAA reveals a weakly resolved 5NAA molecule bound in the active site (Figure 14b). This result was unexpected because no binding was detected by ITC (Figure 13c). This result indicates that while 5NAA binding is weakened, binding can be driven with high

excess of 5NAA, with stabilizing interactions from the intact R289 and R373 (Figure 14a).

3.3 Progress toward understanding substrate loading to active site

As a first attempt to test the hypothesis that substrate loading is mediated by Loop 1, I mutated Arg 98 on this loop to Ala (Figure 15a). After expression and purification of R98A, spectrophotometric assay was used to assess the activity of R98A by following the depletion of 5NAA and generation of 5NSA. The R98A variant showed weak activity compared to wild-type enzyme, barely significant compared to the negative control. This result indicates that R98, over 6.5 Å from the catalytic site (Figure 5), can still affect catalysis.

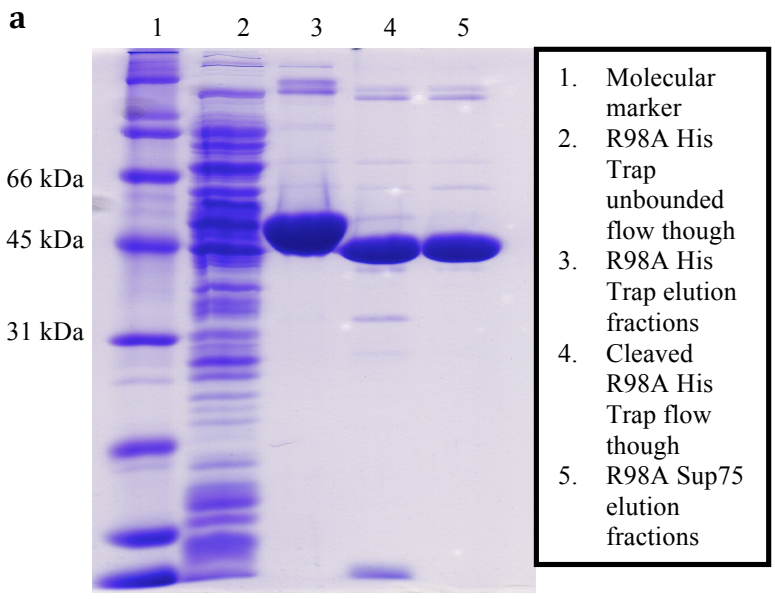

b

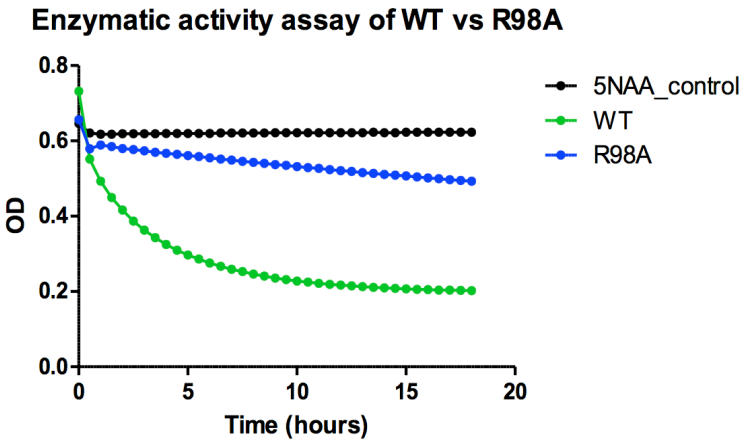

Figure 15: Characterization of 5NAA-A R98A. (a) Gel image of 5NAA-A R98A. (b) Effect of Zn^{2+} on 5NAA-A WT (green) and R98A (blue) activities as measured by 5NAA depletion and 5NSA formation.

To confirm whether any product was generated, mass spectrometry analysis of the assay end-point product was conducted (Bioanalytical Mass Spectrometry Facility). Indeed, evidence for both 5NAA and 5NSA were obtained for the reaction with R98A, compared to 5NSA only for WT 5NAA-A (Figure 16).

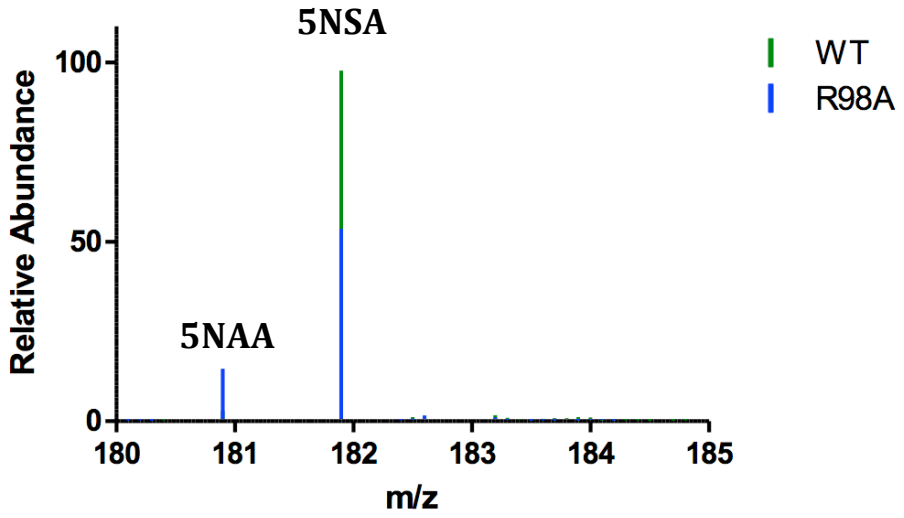

Figure 16: Additional characterization of purified recombinant 5NAA-A R98A. Detection of 5NSA by mass spectrometry. Green: after 5NAA-A WT incubated with metal and substrate for 24 hours as described in methods. m/z = 181.9, composition 5NSA = $C_7H_4O_5N$, and m/z = 180.9, composition 5NAA = $C_7H_5O_4N_2$. Blue: 5NAA-A R98A incubated with metal and substrate.

3.3.1 Binding features of R98A

ITC measurements for 5NAA binding to R98A revealed similar affinity to wild type 5NAA-A (Figure 17, K_d = 1.66±0.139μM). This result indicates that R98 does not impair substrate binding, in agreement with the assay result, but does not rule out the possibility that 5NAA is bound remote from the active site. The stochiometry value was close to 0.5, not 1, however. As suggested for R373A where this was also observed, this could be due to only half of R98A binding sites are able to bind 5NAA.

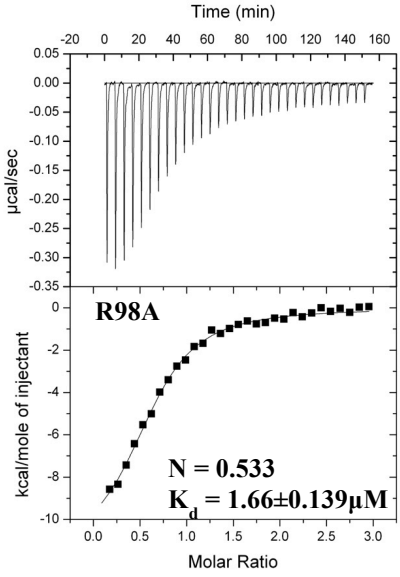

Figure 17: Substrate binding to 5NAA-A E158A and R98A mutants measured by ITC. Representative raw data and plot of integrated heat versus molar ratio with calculated Kd values.

3.3.2 Crystal structure of R98A and 5NAA

The crystal structure of 5NAA bound to R98A was solved to 2.3Å (Table 4) resolution with one octameric molecule in the asymmetric unit. Preliminary refinement indicates that 5NAA is bound at the catalytic pocket through stabilization of R373, Y223, and R289, similar to wild-type 5NAA-A (Figure 18a). Thus, Arg98 does not prevent

substrate binding nor promote an alternative binding site. Interestingly, two conformations of R289 are observed in our structure (Figure 18b). While one monomer in the asymmetric unit is similar to the case of WT 5NAA, in other monomers a favorable cation-π interaction between R289 and F99 on loop 1 is observed, leaving the nitro group poorly stabilized in the active site and missing a key element needed for stabilizing the Meisenheimer complex. This occurs because of a conformational change in loop 1 that repositions this region of the protein (Fig. 18b).

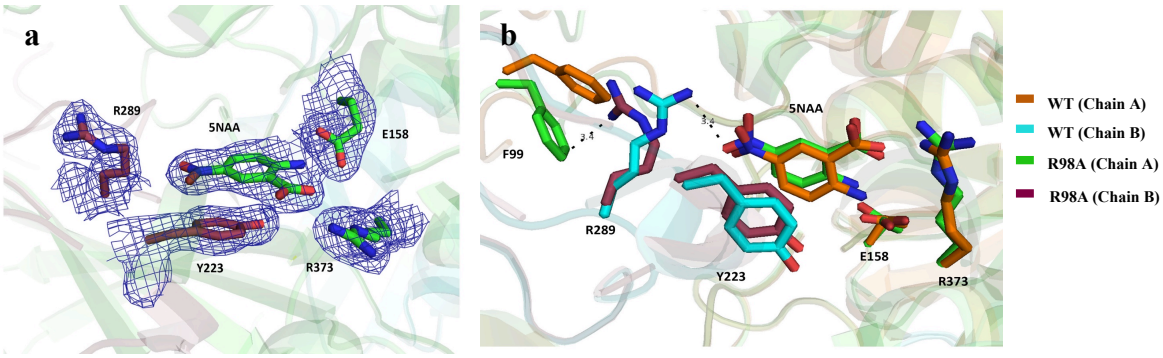

Figure 18: Structure of substrate coordination and electron density map of 5NAA-A R98A. (a) Electron density for 5NAA-bound 5NAA-A R98A. $2F_o - F_c$ electron density (blue) is contoured at 1.0 σ. (b) Superposition of substrate-bound 5NAA-A WT and R98A.

CHAPTER 4

CONCLUSIONS AND DISCUSSION

The 5NAA assisted-metal ion cofactor loading in 5NAA-A constitutes a novel mode of activation for a metalloenzyme. Our structure of 5NAA bound to Zn^{2+} (figure 4) reveals a 2:1 ratio, with coordination of Zn^{2+} via the carboxylate substituents on 5NAA. This result confirms our speculation that electron-withdrawing nitro group on 5NAA causes the *para*-amino substituent to be a weak ligand, so that metal ion complexation in solution instead involves the carboxylate substituent. In the enzyme, however, 5NAA is bound to Zn^{2+} in a 1:1 ratio via the amino substituent and the carboxyl group is stabilized by Arg373 (Figure 3). How this conformational change occurs remains a mystery.

This thesis provides the thermodynamic contribution to each residue in the catalytic center. For metal binding residues, ITC binding assays indicate that mutations at H86 and N124 would not affect substrate binding. However, lower ligand to enzyme ratio, N values, obtained in 5NAA to N124D indicates lower enzyme active concentration during ITC experiments. For substrate binding residues, 5NAA binds considerably more weakly without the stabilization of R289 and R373, and no binding affinity was detected without Y223, which provides π-π stacking interaction with the substrate. All ITC experiments of 5NAA to R373A, Y223A, and R289A showed lower N values compared to that of WT 5NAA-A, suggesting that only partial molecules in the 5NAA-A octamer can bind 5NAA in this variant. By removing functional group E158, we observed that 5NAA binds tighter to the enzyme due to the removal of the negatively charged carboxyl group, which would repel the negatively 5NAA substrate.

Finally, we identified R98, the residue outside the catalytic center we predicted most likely to stabilize the nitro group of the 5NAA substrate along its path to the catalytic pocket of 5NAA-A. Unfortunately, Arg98 did not prevent substrate binding nor drive 5NAA to an alternative binding site. The main change was a repositioning of loop 1 by generating a favorable cation-π interaction between R289 and F99. This alternate arrangement results in slowed catalysis, demonstrating a role in properly positioning the substrate in the active site.

Further studies are required to clarify precisely how the metal ion is delivered to 5NAA-A as well as which metal ion is preferred in biology. We speculate that multiple arginine residues on loop1 and surrounding areas will involve the transport of 5NAA. For metal transport, like most of zinc metalloproteinases contain the consensus zinc binding motif sequence HEXXH[11], 5NAA-A contains speculated zinc metal binding sequence $H^{108}EAWH^{112}$ that could assist transportation of metal-binding 5NAA and affect overall hydrolysis[17]. For example, in thermolysin, a zinc metallopeptidase, two histidine residues from $H^{142}ELTH^{146}$ help to chelate a catalytic zinc ion[17]. Another metallopeptidase, mitochondrial processing peptidase, alanine mutants of glutamates around the active sites, which has a putative metal-binding motif, $H^{56}XXEH^{60}$ affects on kinetics and metal binding[11]. Therefore, it is possible that two histidines and a glutamate in the $H^{108}EAWH^{112}$ motif of 5NAA-A are essential for metal binding and 5NAA-A activity.

Finally, our studies also provide methods to study other identified M20 non-peptidase homologs that likely harbor labile metal binding sites and hydrolyze other aromatic substrates of potential environmental or synthetic interest. 5NAA-A provides

functional annotations of sequences for bioinformatics studies, which could expand our understanding of the largely uncharacterized metal-loading enzymes to mitigate environmental impact of nitroanilines and other harmful substrates.

REFERENCES

1. Spain, J. C., Biodegradation of nitroaromatic compounds. *Annu Rev Microbiol.***49**, 523-555 (1995).

2. Ju, K. S. & Parales, R. E. Nitroaromatic compounds, from synthesis to biodegradation. *Microbiol Mol Biol Rev*. **74**, 250-272 (2010).

3. McGuinness, M. & Dowling, D. Plant-Associated Bacterial Degradation of Toxic Organic Compounds in Soil. *International Journal of Environmental Research and Public Health* **6**, 2226 (2009).

4. Silverman, R. B. *Organic Chemistry of Enzyme-Catalyzed Reactions*. **6**, 2nd ed (2002).

5. King, R. R. & Calhoun, L. A., The thaxtomin phytotoxins: sources, synthesis, biosynthesis, biotransformation and biological activity. *Phytochemistry.* **70**, 833-841 (2009).

6. Lerat, S., Simao-Beaunoir, A. M. & Beaulieu, C. Genetic and physiological determinants of Streptomyces scabies pathogenicity. *Mol Plant Pathol.* **10**, 579-585 (2009).

7. Kalyoncu, S., Heaner, D. P., Jr., Kurt, Z., Bethel, C. M., Ukachukwu, C. U., Chakravarthy, S., Spain, J. C. & Lieberman, R. L. Enzymatic hydrolysis by transition-metal-dependent nucleophilic aromatic substitution. *Nat Chem Biol.* **12**, 1031-1036 (2016).

8. Qu, Y. & Spain, J. C. Biodegradation of 5-nitroanthranilic acid by Bradyrhizobium sp. strain JS329. *Appl Environ Microbiol.* **76**, 1417-1422 (2010).

9. Qu, Y. & Spain, J. C. Molecular and biochemical characterization of the 5-nitroanthranilic acid degradation pathway in Bradyrhizobium sp. strain JS329. *J Bacteriol***. 193**, 3057-3063 (2011).

10. Maret, W. & Li, Y. Coordination dynamics of zinc in proteins. *Chem Rev.* **109**, 4682-4707 (2009).

11. Menach, E., Hashida, Y., Yasukawa, K. & Inouye, K. Effects of conversion of the zinc-binding motif sequence of thermolysin, HEXXH, to that of dipeptidyl peptidase III, HEXXXH, on the activity and stability of thermolysin. *Biosci Biotechnol Biochem.* **77**,, 1901-1906 (2013).

12. Otwinowski, Z. & Minor, W. Processing of X-ray diffraction data collected in oscillation mode. *Methods Enzymol***. 276**, 307-326 (1997).

13. McCoy, A. J., Grosse-Kunstleve, R. W., Adams, P. D., Winn, M. D., Storoni, L. C. & Read, R. J. Phaser crystallographic software. *J Appl Crystallogr***. 40**, 658-674 (2007).

14. Emsley, P., Lohkamp, B., Scott, W. G. & Cowtan, K. Features and development of Coot. *Acta Crystallogr D Biol Crystallogr.* **66**, 486-501 (2010).

15. Adams, P. D. *et al*. PHENIX: a comprehensive Python-based system for macromolecular structure solution. *Acta Crystallogr D Biol Crystallogr***. 66**, 213-221 (2010).

16. Moriarty, N. W., Grosse-Kunstleve, R. W. & Adams, P. D. Electronic Ligand Builder and Optimization Workbench (eLBOW): a tool for ligand coordinate and restraint generation. *Acta Crystallogr D Biol Crystallogr***. 65**, 1074-1080 (2009).

17. Kitada, S. *et al*. Glutamate residues required for substrate building and cleavage activity in mitochondrial processing peptidase. *J Biol Chem***. 273**, 33547-33553 (1998).

18. Ju, K. S. & Parales, R. E. Nitroaromatic compounds, from synthesis to biodegradation. *Microbiol Mol Biol Rev*. **74**, 250-272 (2010).